Applied Surface Science Advances 6 (2021) 100146

Contents lists available at ScienceDirect

Applied Surface Science Advances

journal homepage: www.sciencedirect.com/journal/applied-surface-science-advances

Nanolithography-induced exfoliation of layered materials

Alper Özoğul [a], Enrico Gnecco [a,*], Mehmet Z. Baykara [b]

[a] Otto Schott Institute of Materials Research (OSIM), Friedrich Schiller University Jena, 07743 Jena, Germany
[b] Department of Mechanical Engineering, University of California Merced, Merced, CA 95343, USA

ARTICLE INFO

Keywords:
Atomic force microscopy (AFM)
Friction force microscopy (FFM)
Layered materials
Nanotribology
Wear

ABSTRACT

We present a comparative study of nanoexfoliation on bulk, layered materials (MoS_2, WSe_2, HOPG, and mica) conducted via atomic force microscopy (AFM). The samples were scratched by single crystal diamond probes with varying scan velocities and normal forces. Friction forces measured during the scratch tests and post-mortem topography images allow a detailed investigation of nanoexfoliation mechanisms. In particular, while MoS_2, WSe_2, and HOPG undergo nanoexfoliation that is characterized by the peeling of flakes from the surface and crack propagation off the main scratch direction, mica is devoid of such effects, instead forming well-defined wear tracks that involve layer-by-layer exfoliation of terraces separated by monoatomic steps. A comparison of material properties (bending stiffness, interlayer adhesion, and tensile strength) mechanistically explains the differences in nanoexfoliation behavior. Moreover, the velocity dependence of lateral contact stiffnesses is studied to infer the influence of capillary-adhesion-mediated contact aging on nanoexfoliation, revealing a connection to the degree of surface hydrophobicity. Our results contribute to the formation of a physical understanding of the elementary steps involved in wear of layered materials, and hint at the possibility of precise, controlled nanoexfoliation by a careful selection of operational and environmental parameters.

1. Introduction

The field of tribology —which comprises studies of friction, wear, and lubrication— has experienced a "renaissance" in the last few decades thanks to the development of advanced experimental and computational methods that brought physical insight into an area of inquiry that was long dominated by empirical observations [1]. In particular, the utilization of atomic force microscopy (AFM) has greatly simplified the interpretation of tribology experiments, removing complications associated with analyzing data extracted from micro- and macroscopic interfaces that invariably feature "multi-asperity" contacts, whereby the real contact area is not known a priori. In particular, AFM experiments deliver tribological information obtained at the "single asperity" contact geometry established between the sharp AFM probe and the sample surface under investigation, in a fashion that is devoid of the geometric complexities of a multi-asperity contact. Consequently, AFM experiments, often complemented by atomistic simulations, have been extensively used to shed light on fundamental aspects of friction, e.g. in terms of its load, area, speed, and temperature dependence on nanoscopic length scales [2].

While AFM experiments contributed greatly to the formation of a fundamental understanding of friction, the method has also been used to some extent toward the study of wear, a phenomenon of drastic importance for reliability of mechanical systems [3]. Some attempts have been made to move beyond the empirical Archard wear equation (that simply establishes a proportional relationship between wear volume and normal force as well as sliding distance [4]) that is ubiquitously used in macroscopic systems. These include important studies that reveal atomic-scale wear processes in silicon [5,6], as well as related work focusing on hard coating materials such as ultrananocrystalline diamond [7] and diamond-like carbon [8]. This body of work led to the conclusion that wear on nanoscopic length scales is physically a much richer process than that implied by the Archard equation [9], and that more work needs to be done to form a "first principles" view of the phenomenon.

Within this context, studies of wear on layered materials such as graphite and molybdenum disulfide (MoS_2) bear special importance, due to the fact that these materials are often employed in mechanical systems as solid lubricants [10]. While the bulk form of the materials is typically utilized for macroscopic applications, their two-dimensional (2D) variants are being envisioned as solid lubricants for nano- and micro-scale mechanical systems [11]. As such it is somewhat surprising

* Corresponding author.
E-mail address: enrico.gnecco@uni-jena.de (E. Gnecco).

https://doi.org/10.1016/j.apsadv.2021.100146
Received 11 May 2021; Received in revised form 12 August 2021; Accepted 12 August 2021
Available online 21 August 2021

that the number of nanoscopic wear studies performed on layered materials (either in bulk or 2D form) via AFM are quite low compared to friction work; some highlights can be found in Refs. [12–16]. Importantly, by way of atomistic simulations and AFM experiments performed on single-layer graphene on a platinum substrate, it has been determined that increasing normal loads during sliding lead first to the plastic deformation of the platinum substrate, which is followed by the rupture of graphene, accompanied by a sizeable increase in friction forces [12]. The role of step edges in enhancing wear on graphene has also been investigated [16]. More recent work performed on MoS_2 revealed the tearing and exfoliation of flakes from the surface after a threshold normal load is reached during scratching, whereby the tearing direction could be related to specific crystallographic orientations of the substrate [13]. The fracture [17] and fatigue [18] behavior of layered materials, with relevance to wear, have also been the subject of recent scientific attention.

Motivated by the studies described above and the lack of a mechanistic understanding of processes that dictate the early stages of wear on different layered materials, we present here a comparative set of AFM-based nanoexfoliation experiments performed by scratching single crystal diamond probes on bulk samples of MoS_2, synthetically-grown tungsten diselenide (WSe_2), highly oriented pyrolytic graphite (HOPG), and muscovite mica. In this way we have included in our study two transition metal dichalcogenides (MoS_2 and WSe_2) in natural and artificial forms, respectively, and a layered material (muscovite mica) which, while used more as a filler than a lubricant in tribological applications, finds large use as a substrate in AFM experiments [19]. Our results demonstrate a drastically different nanoexfoliation behavior for mica when compared with the other three materials, among which HOPG stands out by the formation of significantly large flakes during nanoexfoliation. The results are explained by a comparative analysis of material properties including bending stiffness, interlayer adhesion, and tensile strength. While our results contribute to the goal of understanding the basics of wear initiation on layered materials, they also imply the possibility of nanoscale shaping by a precise control of operational and environmental parameters that can, for instance, be utilized in conjunction with spontaneous tearing and peeling effects [20].

2. Materials and methods

Nanoexfoliation experiments were conducted in contact-mode AFM, by way of single crystal diamond tips with nominal radii $r \approx$ 5-10 nm attached to rectangular cantilevers with spring constant values of $k \approx 40$ N/m (*AIST-NT, D300*). Similarly to the experimental procedure followed in Ref. [13], we have used the same tips for both scratching the surfaces in contact mode and imaging the resulting nanostructures in tapping mode. For each experiment, the sample was scanned in a single line with normal forces (F_n) ranging from 2 to 3 μN, which is the maximum force that can be applied with the instrumental setup used in this work (*JPK Instruments, NanoWizard 4*). Scan velocities (v) ranged from 10 nm/s

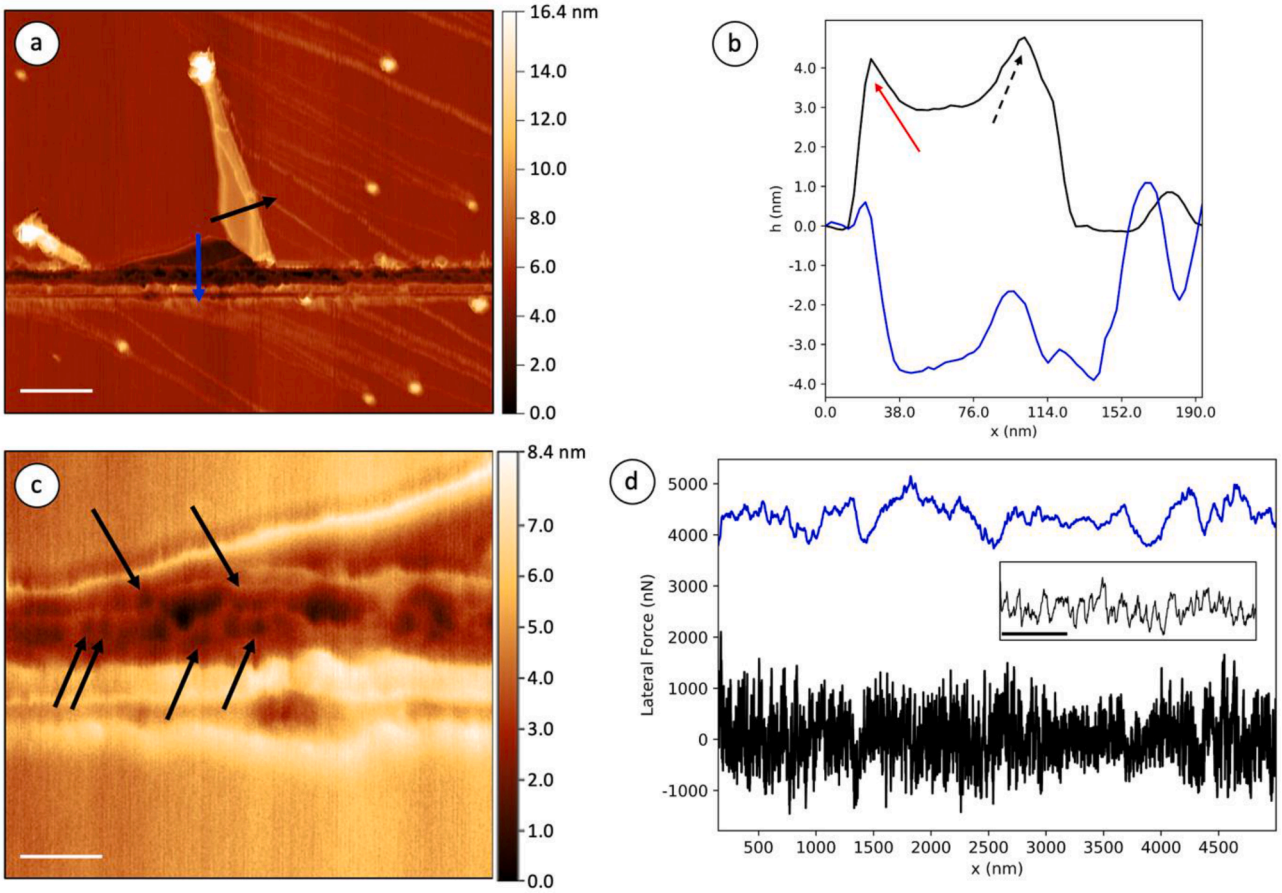

Fig. 1. Nanoexfoliation experiments on MoS_2. (a) Post-mortem topography of the MoS_2 surface, showing layers peeling off the wear track as a result of scratching the surface with $F_n = 3$ μN and $v = 10^{3.5}$ nm/s. (b) Topography profiles taken from the lines indicated with arrows in (a), showing that ~5 layers are removed and folded over the pristine surface, together with the formation of wrinkles (red arrow) and folds (black dashed arrow). (c) High-resolution topography image of the wear track showing indentations (black arrows) that correspond to the spikes in the lateral deflection signal taken during scratching (d). (d) Lateral force experienced by the tip during scratching, where the stick-slip component is shown in black, and the baseline is shown in blue. Inset shows a zoom-in on the stick-slip component. Scale bars correspond to 200 nm in (a), 50 nm in (c), and 100 nm in the inset of (d) (For interpretation of the references to color in this figure legend, the reader is referred to the web version of this article.).

−the lowest velocity with which features on the order of ~10 nm can be sampled in the lateral force signal− to 10^4 nm/s. MoS_2, synthetically-grown WSe_2, ZYB-quality HOPG, and muscovite mica samples were obtained from commercial sources (*HQ Graphene, NanoAndMore*, and *SPI Supplies*). Normal and lateral force calibrations of the cantilevers were performed according to established standards in literature [21,22].

3. Results and discussion

3.1. MoS_2

Bulk MoS_2 substrates were scratched for a length of 5 μm with normal forces of 2.5 μN and 3 μN, and with logarithmically increasing scan velocities in arbitrary crystallographic directions. As demonstrated representatively in Fig. 1, a ~50-nm-wide groove has formed after scratching the surface with $F_n = 3$ μN and $v = 10^{3.5}$ nm/s. As the contact diameter between the tip and the sample is estimated to be only ~9 nm via Hertz theory, this observation implies that the exfoliation process involves cracks propagating off the wear track, as reported for monolayer MoS_2 previously [13,23]. It can also be seen in Fig. 1a that as the AFM tip moves on the surface, multiple layers are removed from the sample in steps and folded back onto the pristine MoS_2 surface. Height profiles taken inside the groove and on the peel (Fig. 1b) show that a total of 5 layers (~ 3 nm) of MoS_2 were removed, and demonstrate the formation of wrinkles and folds ranging from 0.5 to 1 nm in height during the exfoliation process. High resolution post-mortem AFM images of the scratches (Fig. 1c) reveal the formation of repeated indentations with a diameter of ~10 nm in the wear track, reminiscent of a stick-slip like motion. Lateral forces experienced by the tip during nanoexfoliation (Fig. 1d) indeed show that there are two distinct behaviors; a stick-slip motion with a period of ~10 nm that coincides with the average spacing of the indentations made on the surface inside the wear track (shown in black), and a "baseline" (extracted from the raw lateral force signal by low-pass filtering) that follows the topography of the larger peels.

3.2. WSe_2

The experiments on WSe_2 were performed on a single crystal that was grown synthetically, with known crystallographic orientation of crystal edges. This allowed the sample to be scratched in directions that can be related to specific crystallographic directions. As previously seen for MoS_2, the wear behavior of WSe_2 is also strongly anisotropic, whereby cracks propagate off the wear track along the zigzag (ZZ) directions as the sample is being scratched in the armchair (AC) direction (Fig. 2). Another advantage of using synthetically grown crystals is that the sample comprises large, flat terraces, which allows nanoscratches with a larger range of parameters to be performed. When nanoexfoliation tests were conducted along the ZZ and AC directions with varying velocities (Fig. 3), it was seen that (i) the lateral contact stiffness (k) does not depend on velocity and (ii) the average value of the lateral contact stiffness is significantly different in the ZZ and AC directions (k_{ZZ}= 131 N/m and k_{AC} = 86.5 N/m, respectively). While (i) can be tentatively attributed to the hydrophobicity of the surface (please see Section 3.5 for the related discussion) [24,25], the lateral contact stiffness values measured for the ZZ and AC directions in (ii) exhibit an inverse relation with tensile strength (15.05 GPa and 24.70 GPa, for the ZZ and AC directions, respectively [26]). This observation of an inverse relationship between tensile strength and lateral contact stiffness is seen to be generally true for the materials investigated in this study (please see Section 3.5 for the related discussion).

3.3. HOPG

Nanoexfoliation experiments on HOPG show results that are similar to the other van-der-Waals solids investigated above (MoS_2 and WSe_2), as seen in Fig. 4. One particular difference is that layers can be exfoliated

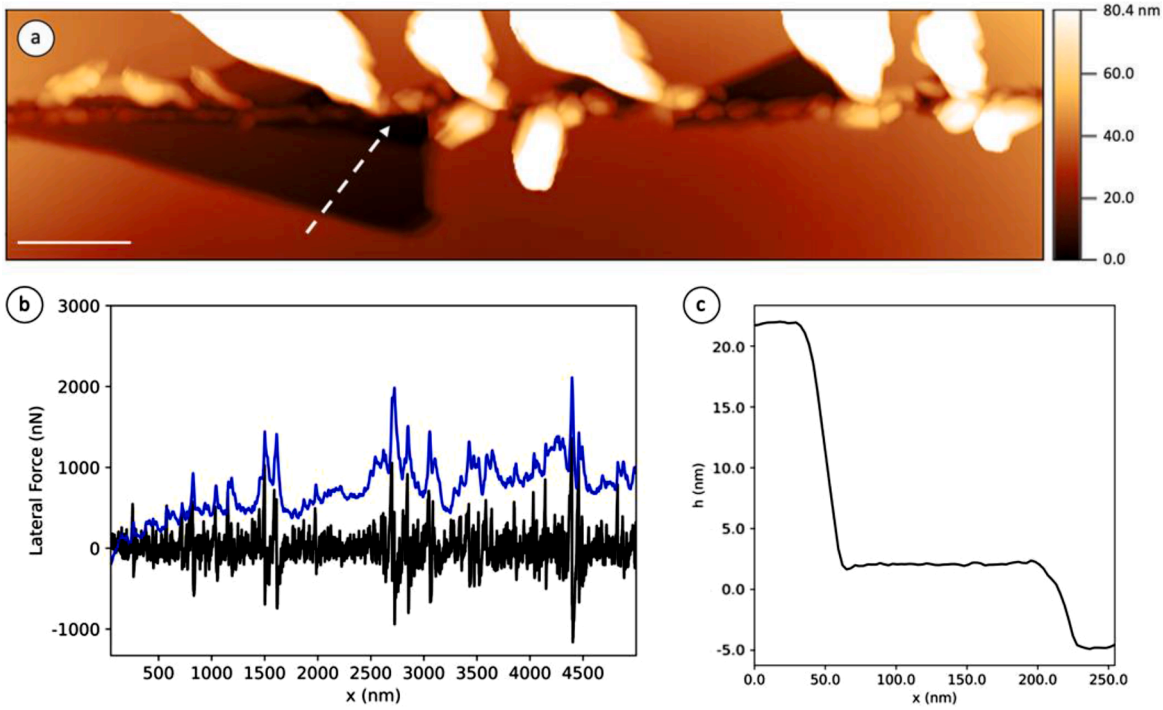

Fig. 2. Nanoexfoliation experiments on WSe_2. (a) Post-mortem topography after scratching the surface with $F_n = 3$ μN and $v = 10^2$ nm/s in the armchair direction showing highly anisotropic crack propagation in the zigzag direction and leaf-like flakes peeled from the surface. Scale bar corresponds to 200 nm. (b) Lateral force experienced by the tip during scratching, where the stick-slip component is shown in black, and the baseline is shown in blue. (c) Topography profile taken along the white dashed line in (a), showing atomically flat terraces of 20 nm and 27 nm depth from the surface (For interpretation of the references to color in this figure legend, the reader is referred to the web version of this article.).

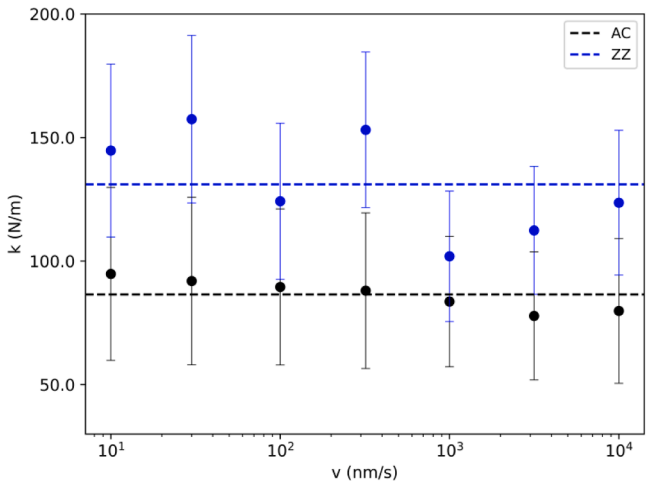

Fig. 3. Lateral contact stiffness (k) during scratching as a function of logarithmically increasing velocities for scratches made along armchair (AC, black) and zigzag (ZZ, blue) directions on WSe_2. Dashed lines indicate mean values (For interpretation of the references to color in this figure legend, the reader is referred to the web version of this article.).

in the form of sizeable flakes that are larger than 1 μm and up to 1.3 μm in lateral size, which is the longest ever detected on any of the materials investigated during the experiments reported here. In the high-resolution AFM image presented in Fig. 4d, it can be seen that the edges of the wear track are jagged, possibly following surface defects along AC and ZZ directions as it has been shown for MoS_2 before [27]. Although there is no clear indication of the crystallographic orientation associated with the scratching direction, the step edge on the left side of the scratch suggests that it's either the zigzag or armchair orientation. Height profiles taken along the wear track (inset in Fig. 4d) show terraces separated by 0.5 - 3.5 nm in the vertical direction, which suggests that progressive removal of the surface down to at least bilayer spacing can be achieved during the scratching process.

3.4. Mica

Mica has a significantly different crystal structure compared to the other materials studied here (MoS_2, WSe_2, and HOPG), whereby a single "layer" consists of multiple atomic sheets with a total thickness of ~1 nm [28]. Although interlayer interactions are significantly weaker than the intralayer binding energy in mica, they are still considerably stronger when compared with interlayer interactions associated with MoS_2, WSe_2, and HOPG [29,30]. This is accompanied by a much more brittle structure with a high bending modulus. Owing to its crystal structure, it is also expected that mica exhibits a smaller degree of in-plane anisotropy than MoS_2, WSe_2, and HOPG [26,31]. When nanoexfoliation experiments are performed on a freshly cleaved mica surface instead of MoS_2, WSe_2, or HOPG, striking differences are found (Fig. 5). First thing to note is that there is no visible crack propagation outside of the wear track, and this is also supported by the fact that the lateral force experienced by the tip during the experiment has a much smoother baseline than MoS_2, WSe_2 and HOPG (Fig. 5b), since no extra work is done to drag and fold peels. Considering the relatively high bending modulus and relatively small tensile strength of mica, exfoliation of long folds is not possible, as the removed layers are expected to break off much easier than the other materials considered here. One implication of this fact is that scratching parameters can be tuned to create very well-defined wear tracks, provided that the sample surface is relatively clean. One example of such a nanoscratch can be seen in Fig. 5, where the exfoliation results in terraces separated by ~0.8 nm in the vertical direction, which is close to the layer spacing of mica [28]. This suggests exfoliation on mica occurs predominantly in single layers. The sudden transitions from one to two monolayer depths and vice versa are possibly due to thermally activated breakup and formation of Si-O bonds, as discussed

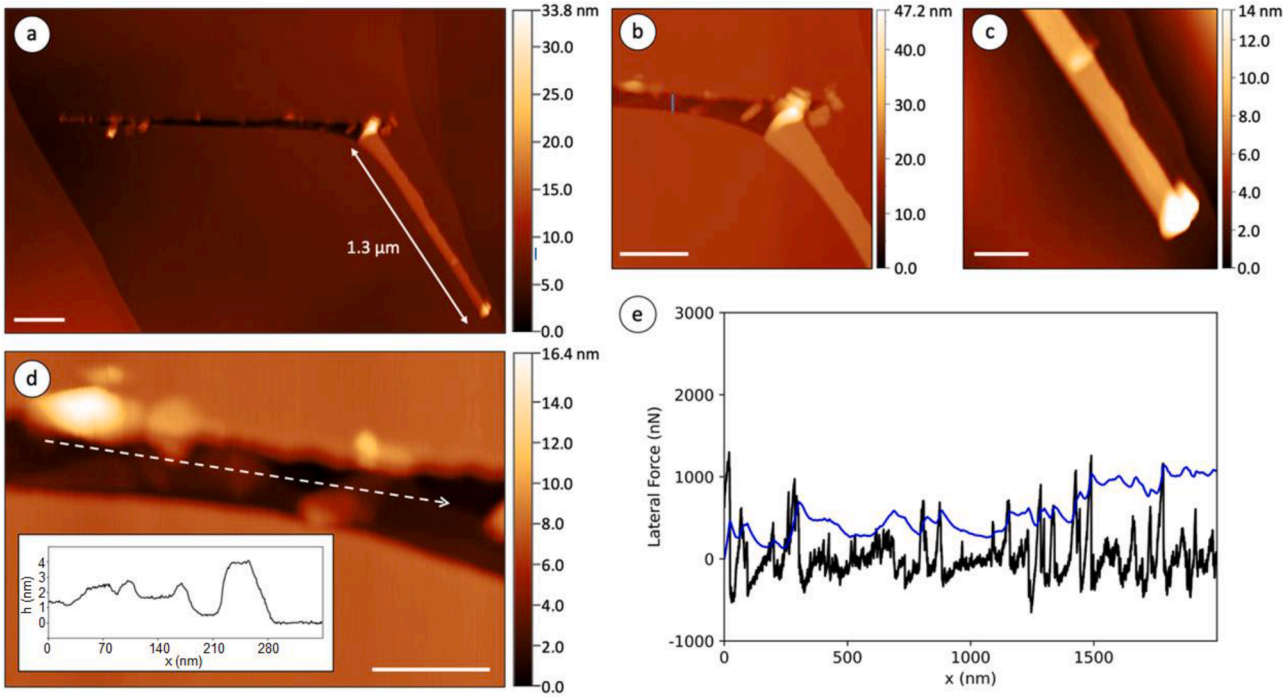

Fig. 4. Nanoexfoliation experiments on HOPG. (a) Post-mortem topography of the HOPG surface after scratching with $F_n = 3$ μN and $v = 10^{3.5}$ nm/s. Scale bar corresponds to 500 nm. (b, c) Zoomed-in topography images of the end of the scratch and the peel, respectively. Scale bars correspond to 200 nm and 100 nm, respectively. (d) High-resolution topography image of the wear track. Inset: Topography profile taken along the dashed white line in (d), showing terraces separated by 0.5 - 3.5 nm in the vertical direction. (e) Lateral force signal corresponding to the topography line profile in the inset of (d). The stick-slip component is shown in black, and the baseline is shown in blue (For interpretation of the references to color in this figure legend, the reader is referred to the web version of this article.).

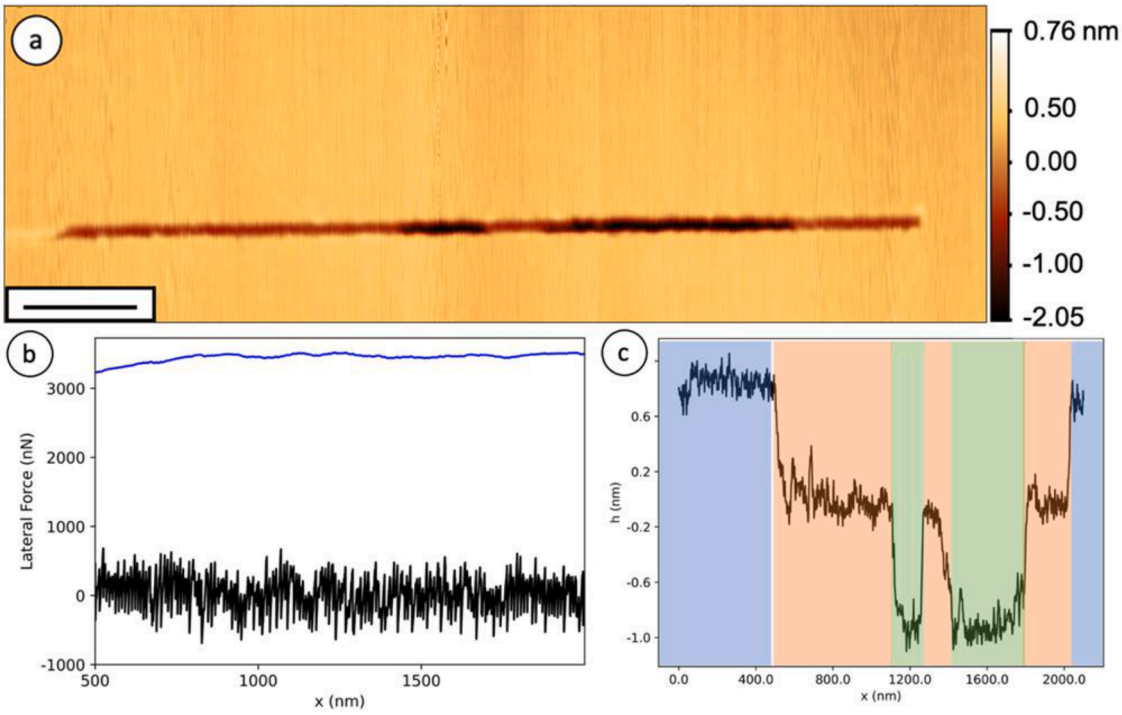

Fig. 5. Nanoexfoliation experiments on mica. (a) Post-mortem topography of the mica surface after scratching with $F_n = 3$ μN and $v = 10$ nm/s. Scale bar corresponds to 200 nm. (b) Lateral force signal corresponding to the scratch in (a), where the stick-slip component is shown in black, and the baseline is shown in blue. (c) Topography profile taken along the wear track in (a), showing clearly resolved terraces separated by ~0.8 nm in the vertical direction. The orange and green areas correspond to regions where one and two monolayers were removed, respectively, whereas the blue areas correspond to regions that remained undamaged (For interpretation of the references to color in this figure legend, the reader is referred to the web version of this article.).

by Kopta *et al.* [28].

3.5. Comparison of Nanoexfoliation Behavior in Layered Materials

From post-mortem topography images, it can be seen that all layered bulk materials studied here besides mica show a similar nanoexfoliation behavior, where flakes peel off the surface in directions off the main wear track, stick to the tip, and after growing up to a certain length, fold back onto the sample outside the wear track while still being partially attached to the substrate on one end. The flake lengths measured in the experiments go up to 1000-1300 nm for HOPG and 200-500 nm for both MoS_2 and WSe_2. No flakes are formed during the nanoexfoliation of mica, which results in well-defined wear tracks (see Supp. Fig. S1 for additional scratch tests). These observations imply that the flakes can only sustain their length up to a critical length l, which could, for instance be determined by the ratio of the tensile strengths of the materials to their bending moduli [32]. In other words, longer flakes would be expected with smaller bending moduli (which makes it easier to peel flakes in the out-of-plane direction from the sample surface) and higher tensile strengths (which conserves the structural integrity of the flake as it is being peeled from the surface). Moreover, a low degree of interlayer adhesion is expected to facilitate the peeling process. The mechanical properties listed in Table 1 support this line of argumentation, whereby HOPG exhibits the highest tensile strength to bending modulus ratio and mica the lowest (and vice versa for interlayer adhesion). Hence, the large flakes for HOPG and no formation of observable flakes on mica. Another possible physical reason for this difference is the formation of covalent bonds between C atoms in the diamond tip and in the top HOPG layers, which are possibly converted into a diamond-like film at high pressures in the GPa range [37, 38]. In this way, the scratching experiments on HOPG reveal characteristic features of adhesive wear (in the peeling process) superimposed on abrasive wear (in the groove formation process). On mica, only the abrasive contribution is present.

Table 1
Mechanical properties of the materials studied in this work.

	Bending Modulus (monolayer) (eV) [33, 34]	Interlayer Adhesion (J m^{-2}) [29,30]	Tensile Strength (monolayer)(GPa) [26, 35, 36]
MoS_2	10.2	0.48	17-27
WSe_2	11.9	0.48	15-25
HOPG	1.87	0.33	110-121
Mica	68.7	0.65	4-9

Another observable in the experiments concerns the normal force threshold for the peeling (i.e. the minimum force required to initiate plastic deformation, F_{thr}). This value also varies from material to material, where we found through our experiments that $F_{thr,MoS2} = 2.5$ μN, $F_{thr,WSe2} = 2.0$ μN, $F_{thr,HOPG} = 3.0$ μN and $F_{thr,mica} \leq 2.0$ μN. This is again in agreement with the tensile strengths of the materials reported in Table 1, which imply that it would require a larger normal force to initiate fracture (and thus, exfoliation) on HOPG when compared with mica, with the two transition metal dichalcogenides (MoS_2 and WSe_2) expected to exhibit intermediate normal force thresholds, in accordance with the experimental results.

Velocity dependence of lateral contact stiffness (inferred from the lateral force (F_L) in the form of $k = \frac{dF_L}{dx}$, which corresponds to the slope of the sticking period of the stick-slip motion of the tip, extracted from the black lines in Figs. 1d, 2b, 4e, and 5b) provides additional clues regarding the nanoexfoliation mechanisms involved in our experiments. In the case of prominent contact aging (where the contact area and thus, the lateral contact stiffness between the tip and the sample increase with time), lateral contact stiffness is expected to decrease logarithmically with velocity. This is because the tip spends a shorter amount of time on a given spot on the surface during the scratching process with increasing scan velocities, thus limiting the extent of contact aging and leading to a decrease of lateral contact stiffness [39]. As the contact aging effect was previously found to vanish under dry atmosphere, it is reasonable to

conclude that capillary condensation at the tip-sample junction mediates contact aging, i.e. a greater degree of condensation per time occurs with slower scan velocities, leading to tip-sample junctions that are harder to deform laterally [13]. This result also implies that hydrophobic surfaces should be less susceptible to capillary-condensation-mediated contact aging and thus not exhibit strong velocity dependence of lateral contact stiffness.

Following up from the discussion above, the results presented in Fig. 6 allow us to evaluate the effect of capillary-condensation-mediated contact aging during nanoexfoliation measurements performed on layered materials. In particular, while mica and MoS_2 exhibit significant drops in lateral contact stiffness with increasing scan velocities, the effect is absent for WSe_2 and HOPG. It should be noted that in the case of HOPG, no exfoliation was observed for scan velocities below 10^3 nm/s, and the lateral contact stiffnesses attained at velocities higher than this value did not change significantly. The observation of a strong contact aging effect for mica is perhaps not surprising considering the hydrophilic nature of the material [25], which would result in the rapid formation of capillary layers at the tip-sample junction. On the other hand, the contrasting behavior of MoS_2 and WSe_2 can be understood when one considers that the experiments on MoS_2 were performed on fresh terraces, immediately after the cleaving of a bulk natural crystal whereas the experiments on WSe_2 were conducted on a CVD-grown synthetic crystal that was not subjected to any cleaning procedure prior to the measurements. As the hydrophobicity of "fresh" surfaces of 2D materials were shown to significantly increase with time due to accumulated contamination from the ambient [40,41], it is natural to expect that the untreated WSe_2 surface investigated here does not exhibit significant capillary-condensation-mediated contact aging whereas the freshly cleaved MoS_2 surface is strongly affected.

Another interesting observation involves the fact that the contact stiffness values measured for the four materials in the region of Fig. 6 that is not affected by contact aging (i.e. at high velocities) generally follow an inverse trend with tensile strength (Table 1), such that HOPG exhibits low and mica exhibits high contact stiffness. This observation is in line with the measurements of contact stiffness along the ZZ and AC directions of WSe_2 (Section 3.2) that showed an inverse relationship to tensile strength. A physical argument that could substantiate these observations involves the idea that it is much easier to form indentations (such as the ones shown in Fig. 1c, which result in stick-slip motion) on the surface of materials with low tensile strength during scratching. This would in turn lead to steeper slopes in the "stick" phase of lateral force traces during scratching due to the tip getting stuck at the indentations, which then manifests as enhanced lateral contact stiffness values.

4. Conclusion

We have presented a comparative study of nanoexfoliation on selected layered materials through experiments performed via AFM. While nanoexfoliation on MoS_2, WSe_2, and HOPG occurred through peeling of flakes from the surface and featured significant crack propagation off the scratches, the nanoexfoliation process on mica was devoid of such effects, with straight grooves forming on the surface in the direction of scratching. Differences in material properties including bending stiffness, interlayer adhesion, and tensile strength were utilized to explain the observed differences in nanoexfoliation behavior. The dependence of lateral contact stiffness on scan velocity was also studied, allowing to form qualitative connections between capillary-adhesion-mediated contact aging and surface hydrophobicity. The results described here provide clues regarding the initial stages of wear in layered materials and open possibilities for precise nanoscale exfoliation utilizing controlled values of normal force, scan velocity and environmental factors such as humidity.

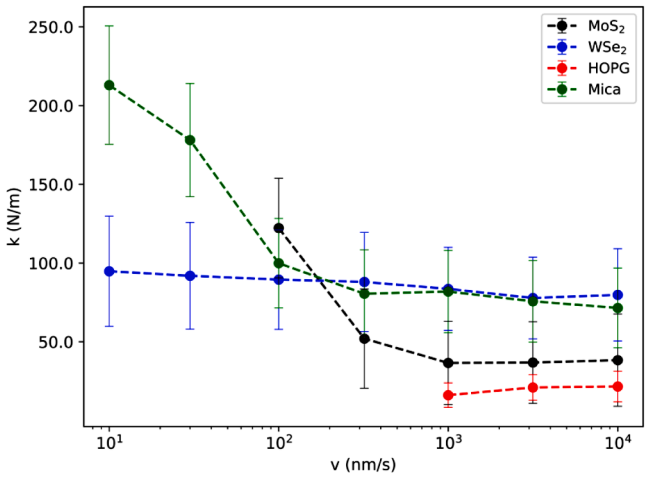

Fig. 6. Dependence of the lateral contact stiffness on scan velocity for MoS_2 (black), WSe_2 (blue), HOPG (red), and mica (green). The WSe_2 plot corresponds to the armchair direction (For interpretation of the references to color in this figure legend, the reader is referred to the web version of this article.).

Declaration of interests

The authors declare that they have no known competing financial interests or personal relationships that could have appeared to influence the work reported in this paper.

Supplementary materials

Supplementary material associated with this article can be found, in the online version, at doi:10.1016/j.apsadv.2021.100146.

References

[1] M. Urbakh, E. Meyer, Nanotribology: The renaissance of friction, Nat. Mater. 9 (2010) 8–10, https://doi.org/10.1038/nmat2599.
[2] A. Vanossi, D. Dietzel, A. Schirmeisen, E. Meyer, R. Pawlak, T. Glatzel, M. Kisiel, S. Kawai, N. Manini, Recent highlights in nanoscale and mesoscale friction, Beilstein J. Nanotechnol. 9 (2018) 1995–2014, https://doi.org/10.3762/bjnano.9.190.
[3] H.P. Jost, Tribology - Origin and future, Wear 136 (1990) 1–17, https://doi.org/10.1016/0043-1648(90)90068-L.
[4] J.F. Archard, Contact and rubbing of flat surfaces, J. Appl. Phys. 24 (1953) 981–988, https://doi.org/10.1063/1.1721448.
[5] T.D.B. Jacobs, R.W. Carpick, Nanoscale wear as a stress-assisted chemical reaction, Nat. Nanotechnol. 8 (2013) 108–112, https://doi.org/10.1038/nnano.2012.255.
[6] B. Gotsmann, M.A. Lantz, Atomistic wear in a single asperity sliding contact, Phys. Rev. Lett. 101 (2008), 125501, https://doi.org/10.1103/PhysRevLett.101.125501.
[7] R.A. Bernal, R.W. Carpick, Visualization of nanoscale wear mechanisms in ultrananocrystalline diamond by in-situ TEM tribometry, Carbon N. Y. 154 (2019) 132–139, https://doi.org/10.1016/j.carbon.2019.07.082.
[8] J. Liu, Y. Jiang, D.S. Grierson, K. Sridharan, Y. Shao, T.D.B. Jacobs, M.L. Falk, R. W. Carpick, K.T. Turner, Tribochemical Wear of Diamond-Like Carbon-Coated Atomic Force Microscope Tips, ACS Appl. Mater. Interfaces. 9 (2017) 35341–35348, https://doi.org/10.1021/acsami.7b08026.
[9] Y. Shao, T.D.B. Jacobs, Y. Jiang, K.T. Turner, R.W. Carpick, M.L. Falk, Multibond Model of Single-Asperity Tribochemical Wear at the Nanoscale, ACS Appl. Mater. Interfaces. 9 (2017) 35333–35340, https://doi.org/10.1021/acsami.7b08023.
[10] T.W. Scharf, S.V. Prasad, Solid lubricants: A review, J. Mater. Sci. 48 (2013) 511–531, https://doi.org/10.1007/s10853-012-7038-2.
[11] D. Berman, A. Erdemir, A.V Zinovev, A.V Sumant, Nanoscale friction properties of graphene and graphene oxide, Diam. Relat. Mater. 54 (2015) 91–96, https://doi.org/10.1016/j.diamond.2014.10.012.
[12] A. Klemenz, L. Pastewka, S.G. Balakrishna, A. Caron, R. Bennewitz, M. Moseler, Atomic scale mechanisms of friction reduction and wear protection by graphene, Nano Lett 14 (2014) 7145–7152, https://doi.org/10.1021/nl5037403.
[13] A. Özoğul, F. Trillitzsch, C. Neumann, A. George, A. Turchanin, E. Gnecco, Plowing-induced nanoexfoliation of mono-and multilayer MoS2 surfaces, Phys. Rev. Mater. 4 (2020), 033603, https://doi.org/10.1103/PhysRevMaterials.4.033603.
[14] B. Vasić, A. Matković, U. Ralević, M. Belić, R. Gajić, Nanoscale wear of graphene and wear protection by graphene, Carbon N. Y. 120 (2017) 137–144, https://doi.org/10.1016/j.carbon.2017.05.036.

[15] L.Y. Lin, D.E. Kim, W.K. Kim, S.C. Jun, Friction and wear characteristics of multi-layer graphene films investigated by atomic force microscopy, Surf. Coatings Technol. 205 (2011) 4864–4869, https://doi.org/10.1016/j.surfcoat.2011.04.092.
[16] Y. Qi, J. Liu, J. Zhang, Y. Dong, Q. Li, Wear Resistance Limited by Step Edge Failure: The Rise and Fall of Graphene as an Atomically Thin Lubricating Material, ACS Appl. Mater. Interfaces. 9 (2017) 1099–1106, https://doi.org/10.1021/acsami.6b12916.
[17] P. Zhang, L. Ma, F. Fan, Z. Zeng, C. Peng, P.E. Loya, Z. Liu, Y. Gong, J. Zhang, X. Zhang, P.M. Ajayan, T. Zhu, J. Lou, Fracture toughness of graphene, Nat. Commun. 5 (2014) 3782, https://doi.org/10.1038/ncomms4782.
[18] T. Cui, S. Mukherjee, P.M. Sudeep, G. Colas, F. Najafi, J. Tam, P.M. Ajayan, C. V. Singh, Y. Sun, T. Filleter, Fatigue of graphene, Nat. Mater. 19 (2020) 405–411, https://doi.org/10.1038/s41563-019-0586-y.
[19] P. Eaton and W. West (2010) "Substrates for AFM", pp. 87–89 in Atomic Force Microscopy. Oxford University Press.
[20] J. Annett, G.L.W. Cross, Self-assembly of graphene ribbons by spontaneous self-tearing and peeling from a substrate, Nature 535 (2016) 271–275, https://doi.org/10.1038/nature18304.
[21] J.E. Sader, J.W.M. Chon, P. Mulvaney, Calibration of rectangular atomic force microscope cantilevers, Rev. Sci. Instrum. 70 (1999) 3967–3969, https://doi.org/10.1063/1.1150021.
[22] D.F. Ogletree, R.W. Carpick, M. Salmeron, Calibration of frictional forces in atomic force microscopy, Rev. Sci. Instrum. 67 (1996) 3298–3306, https://doi.org/10.1063/1.1147411.
[23] S. Wang, Z. Qin, G.S. Jung, F.J. Martin-Martinez, K. Zhang, M.J. Buehler, J. H. Warner, Atomically Sharp Crack Tips in Monolayer MoS 2 and Their Enhanced Toughness by Vacancy Defects, ACS Nano 10 (2016) 9831–9839, https://doi.org/10.1021/acsnano.6b05435.
[24] P.K. Chow, E. Singh, B.C. Viana, J. Gao, J. Luo, J. Li, Z. Lin, A.L. Elías, Y. Shi, Z. Wang, M. Terrones, N. Koratkar, Wetting of mono and few-layered WS2 and MoS2 films supported on Si/SiO2 substrates, ACS Nano 9 (2015) 3023–3031, https://doi.org/10.1021/nn5072073.
[25] M.R. Uhlig, D. Martin-Jimenez, R. Garcia, Atomic-scale mapping of hydrophobic layers on graphene and few-layer MoS2 and WSe2 in water, Nat. Commun. 10 (2019) 2606, https://doi.org/10.1038/s41467-019-10740-w.
[26] J. Li, N.V. Medhekar, V.B. Shenoy, Bonding charge density and ultimate strength of monolayer transition metal dichalcogenides, J. Phys. Chem. C. 117 (2013) 15842–15848, https://doi.org/10.1021/jp403986v.
[27] M.S.R. Elapolu, A. Tabarraei, X. Wang, D.E. Spearot, Fracture mechanics of multi-layer molybdenum disulfide, Eng. Fract. Mech. 212 (2019) 1–12, https://doi.org/10.1016/j.engfracmech.2019.02.027.
[28] S. Kopta, M. Salmeron, The atomic scale origin of wear on mica and its contribution to friction, J. Chem. Phys. 113 (2000) 8249–8252, https://doi.org/10.1063/1.1314376.
[29] K.-T Wan, D.T. Smith, B.R. Lawn, Fracture and Contact Adhesion Energies of Mica-Mica, Silica-Silica, and Mica-Silica Interfaces in Dry and Moist Atmospheres, J. Am. Ceram. Soc. 75 (1992) 667–676, https://doi.org/10.1111/j.1151-2916.1992.tb07857.x.
[30] H. Rokni, W. Lu, Direct measurements of interfacial adhesion in 2D materials and van der Waals heterostructures in ambient air, Nat. Commun. 11 (2020) 5607, https://doi.org/10.1038/s41467-020-19411-7.
[31] G.D. Zartman, H. Liu, B. Akdim, R. Pachter, H. Heinz, Nanoscale tensile, shear, and failure properties of layered silicates as a function of cation density and stress, J. Phys. Chem. C. 114 (2010) 1763–1772, https://doi.org/10.1021/jp907012w.
[32] D.-M. Tang, D.G. Kvashnin, S. Najmaei, Y. Bando, K. Kimoto, P. Koskinen, P. M. Ajayan, B.I. Yakobson, P.B. Sorokin, J. Lou, D. Golberg, Nanomechanical cleavage of molybdenum disulphide atomic layers, Nat. Commun. 5 (2014) 3631, https://doi.org/10.1038/ncomms4631.
[33] J. Zhao, Q. Deng, T.H. Ly, G.H. Han, G. Sandeep, M.H. Rümmeli, Two-dimensional membrane as elastic shell with proof on the folds revealed by three-dimensional atomic mapping, Nat. Commun. 6 (2015) 8935, https://doi.org/10.1038/ncomms9935.
[34] Y.T. Fu, G.D. Zartman, M. Yoonessi, L.F. Drummy, H. Heinz, Bending of layered silicates on the nanometer scale: Mechanism, stored energy, and curvature limits, J. Phys. Chem. C. 115 (2011) 22292–22300, https://doi.org/10.1021/jp208383f.
[35] A. Castellanos-Gomez, M. Poot, A. Amor-Amorós, G.A. Steele, H.S.J. van der Zant, N. Agraït, G. Rubio-Bollinger, Mechanical properties of freely suspended atomically thin dielectric layers of mica, Nano Res 5 (2012) 550–557, https://doi.org/10.1007/s12274-012-0240-3.
[36] F. Liu, P. Ming, J. Li, Ab initio calculation of ideal strength and phonon instability of graphene under tension, Phys. Rev. B - Condens. Matter Mater. Phys. 76 (2007), 064120, https://doi.org/10.1103/PhysRevB.76.064120.
[37] Y. Gao, T. Cao, F. Cellini, C. Berger, W.A. de Heer, E. Tosatti, E. Riedo, A. Bongiorno, Ultrahard carbon film from epitaxial two-layer graphene, Nat. Nanotechnol. 13 (2018) 133–138, https://doi.org/10.1038/s41565-017-0023-9.
[38] P. Ares, M. Pisarra, P. Segovia, C. Diaz, F. Martin, E.G. Michel, F. Zamora, C. Gomez-Navarro, J. Gomez-Herrero, Tunable Graphene Electronics with Local Ultrahigh Pressure, Adv. Funct. Mater. 29 (2019), 1806715, https://doi.org/10.1002/adfm.201806715.
[39] J.J. Mazo, D. Dietzel, A. Schirmeisen, J.G. Vilhena, E. Gnecco, Time Strengthening of Crystal Nanocontacts, Phys. Rev. Lett. 118 (2017), 246101, https://doi.org/10.1103/PhysRevLett.118.246101.
[40] A. Kozbial, X. Gong, H. Liu, L. Li, Understanding the Intrinsic Water Wettability of Molybdenum Disulfide (MoS 2), Langmuir 31 (2015) 8429–8435, https://doi.org/10.1021/acs.langmuir.5b02057.
[41] X. Chen, Z. Yang, S. Feng, T.W. Golbek, W. Xu, H.J. Butt, T. Weidner, Z. Xu, J. Hao, Z. Wang, How Universal Is the Wetting Aging in 2D Materials, Nano Lett. 20 (2020) 5670–5677, https://doi.org/10.1021/acs.nanolett.0c00855.